J. Mol. Biol. (1979) **130**, 451–472

Three-dimensional Reconstruction of the 14-Filament Fibers of Hemoglobin S

GENE W. DYKES, RICHARD H. CREPEAU AND STUART J. EDELSTEIN

Section of Biochemistry, Molecular and Cell Biology
Cornell University, Ithaca, N.Y. 14853, U.S.A.

(Received 21 July 1978, and in revised form 12 February 1979)

The supramolecular structure of hemoglobin S has been studied by electron microscopy and computer-based image reconstruction. Negatively stained fibers prepared by the lysis of sickled cells or the stirring of hemoglobin S hemolysates have been observed to be almost exclusively of the 20-nm diameter form. These fibers have a periodic variation in diameter between the extremes of 18 nm and 23 nm. Computed Fourier transforms of the fibers show a highly complex pattern of reciprocal space maxima, with 30 maxima on 20 layer-lines clearly resolved. The Bessel orders of the maxima were assigned with the aid of a newly developed technique, a combined real-space Fourier-space reconstruction method (REFORM). This method utilizes the filtered image produced by the inverse Fourier transform of the low-resolution maxima to calculate in real space the cross-section of a helical fiber. The REFORM analysis indicated that the fibers have an elliptical cross-section and are composed of 14 hexagonally packed filaments with 10 outer filaments surrounding four inner filaments. On the basis of this cross-section, the Bessel orders of all the maxima were assigned, permitting the calculation of three-dimensional reconstructions by Fourier Bessel synthesis. From these reconstructions details of the location of hemoglobin S molecules of each filament were obtained. Hemoglobin S molecules are staggered in adjacent filaments to produce a closely packed helical structure. Reconstructions of fibers at various stages of disassembly revealed a stable intermediate containing 10 filaments which could be characterized in terms of the loss of two pairs of specific outer filaments. A partially disassembled fiber with only six filaments at positions corresponding to three inner and three outer filaments of the parent structure was also identified. The six-filament structure appears to be produced from the 10-filament structure by the loss of two specific pairs of filaments. Thus pairs of filaments are evidently significant structural units in the stabilization of the complete fibers and the orientation of the molecules in these pairs may be related to the filament pairs known to occur in crystals of hemoglobin S.

1. Introduction

Sickle cell anemia is an hereditary disease that arises from a mutation in the β-globin gene. An A $\rightarrow$ T transition in the second base of the codon specifying the amino acid for the sixth position of the beta chains of hemoglobin results in the substitution of valine for glutamic acid. This replacement, which is on the surface of the molecule, has little effect when HbS† is oxygenated, but in the deoxy conformation HbS has greatly reduced solubility and aggregates into long fibers. These fibers align parallel

† Abbreviations used: Hb, hemoglobin; IHP, inositol hexaphosphate.

0022-2836/79/160451-22 $02.00/0

to each other to form large aggregates which distort the cell membrane. If the molecular contacts of HbS within the fibers could be specified, a rational attempt to design anti-sickling agents might be possible. Toward this end, we are studying the fibers of HbS with electron microscopy and computerized image reconstruction techniques.

There appear to be at least two types of fibers: one composed of six filaments or strands of HbS molecules and one composed of 14 filaments. Finch *et al.* (1973) showed that the six-stranded fibers, which have a diameter of 17 nm, are formed with HbS molecules of adjacent filaments in longitudinal register to give the appearance of a stack of six-membered rings. This fiber has also been examined by Ohtsuki *et al.* (1977). The 14-stranded type, which has an approximate average diameter of 20 nm, was formerly thought to be a hollow structure with only eight filaments (Josephs *et al.*, 1976; Crepeau *et al.*, 1977) prior to our discovery of inner core filaments (Dykes *et al.*, 1978). This is quite likely the same form observed by other investigators (Stetson, 1966; White, 1968; Bertles *et al.*, 1970) although the reported diameters appear to have been underestimated, perhaps by measuring single fibers (where edges are indistinct) rather than center-to-center distances between adjacent fibers. This form of the fiber is much more complicated than the six-stranded type, and mere inspection of its micrographs and their optical transforms is inadequate to deduce its structure. Advances in fiber preparation techniques and the combination of real-space and Fourier-space reconstruction methods have made the determination of the 20-nm diameter fiber structure possible.

There are several methods of preparing HbS fibers for electron microscopy. Thin sections from embedded sickled cells have the greatest probability of revealing physiologically significant structures, but with present techniques they are unsuitable for high-resolution studies. Negative staining techniques are complicated by the fact that the optimal concentration of HbS on the grids is far below the concentration at which fibers spontaneously dissociate. Sickled cells can be lysed with distilled water, and then stained and dried, but this perhaps allows time for the fibers to rearrange. Since we feel this procedure should be done as quickly as possible, we combine lysing and staining in one step (Josephs *et al.*, 1976). By lysing with 1% phosphotungstic acid the procedure is much faster, and the presence of stain potentially stabilizes the existing fibers. It is also possible to study fibers prepared from cell-free solutions of HbS. When a chilled solution of deoxy HbS above the minimum gelling concentration is warmed, the molecules of HbS assemble into fibers and a gel is formed. Stirring HbS solutions during the warming stage inhibits gel formation (Pumphrey & Steinhardt, 1976) and results in production of bundles of fibers (Crepeau *et al.*, 1977). After dilution of the fibers onto the grid, excess HbS must be washed off. A balance must be struck between thorough washing, necessary for high-resolution images, and disrupting the fibers by excessive washing. Since we have found no difference in the structure of the fibers from all preparations, the stirred HbS solution technique is important because it provides a greater number of fibers which are clean and undisrupted over a sufficient length to be computationally useful. From blood samples of dozens of donors we have observed the 20 nm fibers in embedded cells and preparations from lysed cells, gels and bundles, whereas the 17 nm fibers have only been reported in a limited number of lysed cell preparations (Finch *et al.*, 1973; Josephs *et al.*, 1976; Ohtuski *et al.*, 1977). Therefore we conclude that the 20 nm fibers are likely to correspond to the predominant form of the fibers in circulating sickled cells, particularly since recent measurements on cross-sections of fibers in sectioned sickled cells are consistent with the 14-stranded

structure in terms of diameters (Crepeau *et al.*, 1978) and, when tannic acid is used in the embedding, resolvable detail (Garrell *et al.*, 1979).

Progress in image reconstruction has been as essential to our work as improvements in fiber preparation. DeRosier & Moore (1970) presented a Fourier method for the three-dimensional reconstruction of biological structures with helical symmetry from their two-dimensional electron micrograph images. The method described was designed for use on a large multi-user computer where input is accomplished mainly *via* punched cards and output comes primarily from a line printer. For this work we implemented the process on our laboratory minicomputer, which resulted in a very convenient image reconstruction system which includes the advantages of graphic output and operator interaction that greatly enhanced the speed of our work. In addition, the complexities of the structure of the HbS fibers led us to develop another method for determining structure from projected views based on real-space reconstructions. A real-space method called algebraic reconstruction technique (ART) was introduced by Gordon *et al.* (1970). Among the many improved algorithms presented since then is the extended field iterative reconstruction technique (EFIRT) developed by Crowther & Klug (1974). Employing EFIRT, we designed a combined real-space Fourier-space reconstruction method, REFORM, for determining the cross-section of a helical structure. Use of the REFORM procedure was essential in our determination of the general structure of the HbS fibers. The general conclusions of our studies leading to the description of the 14-stranded structure have been described recently (Dykes *et al.*, 1978) and the details of the analysis will be presented more fully here.

2. Materials and Methods

(a) *Fiber preparation*

Whole blood from various donors homozygous for sickle cell disease was washed with 1% NaCl and the erythrocytes separated by centrifugation. The washing and centrifugation were repeated twice. Portions were set aside for lysed cell studies, and HbS was obtained from the remainder by lysing with distilled water and purified by centrifugation from NaCl solutions to remove membranes. Hemolysates were concentrated by vacuum dialysis to a final concentration of 18 mM-heme and adjusted to pH 6·5, 0·05 M-phosphate, and 5 mM-inositol hexaphosphate by dialysis. Whole cells were adjusted to pH 6·5. No detectable difference was observed for fibers prepared at physiological pH compared to those prepared at pH 6·5. However, the fibers are evidently more stable at pH 6·5, since they are generally in greater abundance on electron microscope grids at this pH. Therefore, pH 6·5 was used routinely. Although IHP had been believed to influence the structure of the fibers (Crepeau *et al.*, 1977), we now realize that IHP only aids in the stabilization of the fibers, but does not alter its general structure. Fibers with no detectable differences can be observed with and without IHP, but their abundance (and hence the likelihood of finding well preserved fibers with high-resolution detail) is much lower in the absence of IHP.

Samples of hemolysates were deoxygenated in an ice bath under a nitrogen atmosphere by stirring slowly to prevent bubble formation. The samples were then transferred to a 35°C water bath and stirring was continued until a color change due to light scattering indicated the onset of the formation of bundles of fibers. Samples of cells were deoxygenated in an ice bath under a stream of nitrogen and transferred to a 35°C water bath to induce sickling.

For electron microscopy, grids coated with either carbon or Formvar-backed holey films were used. A solution of 1 to 2% phosphotungstic acid and 5 mM-IHP was bubbled with nitrogen and used as both a negative stain and a lysing agent. In a nitrogen atmosphere a small quantity of either sickled cells or bundles was daubed onto the edge of a

grid. A drop of phosphotungstic acid was then applied to a grid which was then tilted, allowing the fibers to flow onto the surface of the grid. The acid was drawn off by touching a tissue to the edge of the grid at a point opposite to where the sample was applied. Washing was accomplished by repeating the procedure but without tilting the grid, to prevent additional spreading from the sample. Grids were then dried in a stream of nitrogen gas. A Philips EM301 was used throughout this investigation, and minimal dosage techniques (Williams & Fisher, 1970; Crepeau *et al.*, 1977) were employed. Micrographs were taken at a magnification of 68,000 × .

(b) *Computer system hardware*

Our laboratory computer system consists of a Data General Nova 1200 with 32K 16-bit word memory, a floating-point hardware unit, 2 disk drives with 2·5 megabyte storage capacity each, a magnetic tape drive, a high-speed printer, a Tektronics model 4014-1 graphics terminal, and a Syntex AD-1 autodensitometer. This configuration has proven very satisfactory for on-line image processing. Disks provide storage for programs, temporary storage of data, and auxiliary run-time array space. Magnetic tapes provide permament data storage and disk backups. The graphics terminal is used for interactive communication and graphic displays of data, and the high-speed printer provides printed output. Some programs were run on a recently added Eclipse computer.

(c) *Computer system software*

Collection programs were supplied by Syntex and modified to suit our particular applications. The image processing procedure is essentially that of DeRosier & Moore (1970). Some of our programs were patterned after Fortran program listings kindly supplied to us by the MRC Laboratory, Cambridge. Major enhancements to their method include programs for interactive location of vertices for boxing the image, an improved method of floating to calculate the perimeter density exactly for polygonal boxes of arbitrary shape, a matrix transposition program based on that of Eklundh (1972), interactive mask creation for image filtration, and the REFORM programs (described in Results). The fast Fourier transform (FFT) subroutine was supplied by Floating Point Systems, Inc. All other programs were designed by us and written in either Fortran or assembly language.

(d) *Optical diffraction and densitometry*

An optical diffractometer from Lansing Research Corp. was used to screen the large number of micrographs, and plates with acceptable diffraction patterns were selected for densitometry. The Syntex Autodensitometer offers a choice of 4 apertures. The aperture we selected for measuring optical density was a square, 0·003 cm on a side, which corresponds (at magnification 68,000 ×) to a spacing of 0·44 nm on the fibers. Data were collected every 0·003 cm, thus fully sampling the area of a micrograph without overlap in measurement. This set of optical densities was then converted to the sampling frequency desired for computation by averaging 9 (3 × 3) data points together, to give a final sampling frequency of approx. 1·3 nm.

3. Results

The predominant fibers of HbS have a periodic variation in apparent diameter of 21 nm to 27 nm as shown in Figure 1(a). These measured values are necessarily approximations due to the uncertainty in defining the edges of the fibers, and are certainly greater than the actual diameter of a fiber due to flattening on the surface of the grid. Estimations of the degree of flattening have been made by measuring the diameters of fibers photographed at different angles on a tilting stage. Tilting (parallel to the fiber axis) resulted in an apparent decrease in average diameter which was used to calculate the degree of flattening from geometric considerations (Josephs & Borisy, 1972). Flattening of 15% was estimated, reducing the apparent diameter to 18 nm

and 23 nm for the minimum and maximum diameters. The distance between successive regions of maximum diameter falls in the range 145 nm to 180 nm, and this length represents a 180° turn of the filaments of the helix. Regions of maximum diameter are associated with the appearance of five parallel striations. Regions of four parallel striations are found between the areas of minimum and maximum diameter. By observing the movement of these striations relative to the background in a series of micrographs taken on a tilting stage, the helical sense of these striations was determined to be right-handed†.

The three fibers that provided most of the detailed data for our analysis are shown in Figure 1. Fiber (a) was prepared by cell lysis and fibers (b) and (c) were prepared from stirred HbS solutions. Based on visual appearance and optical transforms, these three are representative of the vast majority of fibers we have observed. These were selected from among hundreds of micrographs as being the most suitable for computer analysis, since most fibers are unsuitable because of non-linearity, obviously discontinuous structure, interference from neighboring fibers, or uneven staining.

The fibers were characterized initially by optical diffraction as illustrated by the diffraction pattern in Figure 2(b). However, the structure of the fibers cannot be determined through the use of optical transforms alone for a number of reasons. As in all optical transforms, the phase information of the maxima is lost, without which the assignment of odd or even Bessel orders to the maxima is difficult. Many of the reflections near the equator are also obscured by the spikes in the transform produced by the edges of the mask. The most serious problem is that the symmetry of this helix is such that many maxima are relatively weak and cannot be distinguished from noise in any individual optical transform. Presumably this situation arises from the fact that the HbS molecules in the fibers are at many non-equivalent sets of locations, leading to numerous maxima, each of which tend to be weak compared to the more typical cases in which all molecules are at equivalent positions. The primary purpose of optical diffraction, then, is to screen the large number of micrographs for those fibers whose optical transforms indicate promise for the more time-consuming computer transformation. This was accomplished by viewing the optical transforms of a great number of plates until a consistent pattern was apparent. The reflections appeared to fall on a reciprocal lattice with a cluster of maxima in the near-equatorial region, clusters of maxima in the region of the transform corresponding to a reciprocal spacing of approximately 1/60 Å, and a set of reflections in the 1/30 Å region (Crepeau *et al.*, 1977). Individual transforms were then compared to this pattern and plates that displayed all these maxima and showed good symmetry across the meridian were chosen.

More definitive data on the fibers were then obtained from computed transforms of digitized micrographs using Fourier methods. Computed transforms offer many advantages over optical transforms. The phase information of the reflections can be determined, the spikes arising from the borders of the image can be mathematically suppressed, creating masks for inverse transforms is much easier, and three-dimen-

† The handedness of the helix was determined by first establishing the relationship between the movement of a fiber on the goniometer stage and the observed differences in the images recorded on the micrographs. With the Philips EM301 at 68,000× magnification, translation of the stage parallel to its rotation axis and observation of the movement of the image determined the direction of the rotation axis at the image plane. Fibers with z-axes parallel to the rotation axis were photographed at various tilt angles. A positive rotation with respect to the z-axis results in movement of the long striations in the negative z direction, a characteristic of right-handed helices.

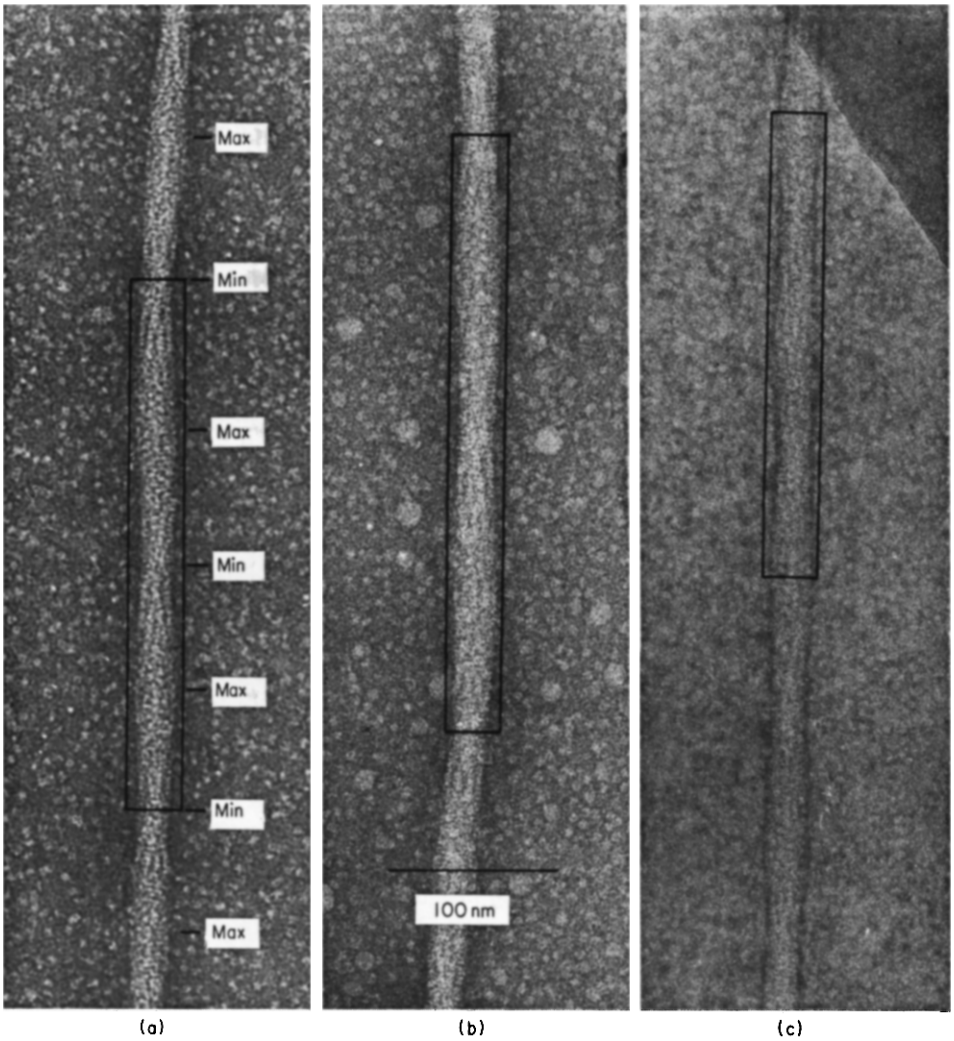

FIG. 1. Electron micrographs of 3 fibers for which 3-dimensional reconstructions were computed. The area used for the computed transforms is outlined for each fiber. The length of this area is chosen to be equivalent to a 360° rotation of the filaments. The points of minimum and maximum diameter are indicated for fiber (a).

sional Fourier synthesis is possible using the numeric Fourier coefficients of the transform. Our experience with computed transforms, however, leads us to believe that sampling a length of helix insufficient for optimal results is not always self-evident and can lead to erroneous conclusions. Our best fibers from lysed cells rarely exhibited a stable structure longer than 200 nm. Therefore, we originally chose to select for our transforms a region of the fibers between two points of minimum diameter, a length of approximately 150 nm. The computed transforms agreed quite well with their optical equivalents, so there was little reason at first to suspect that our sampling area was insufficient. The phases were determined to be even for the near-equatorial maxima and the 1/30 Å maxima, and to be odd for the 1/60 Å maxima. These data were consistent with an eight-stranded fiber with the 1/60 Å

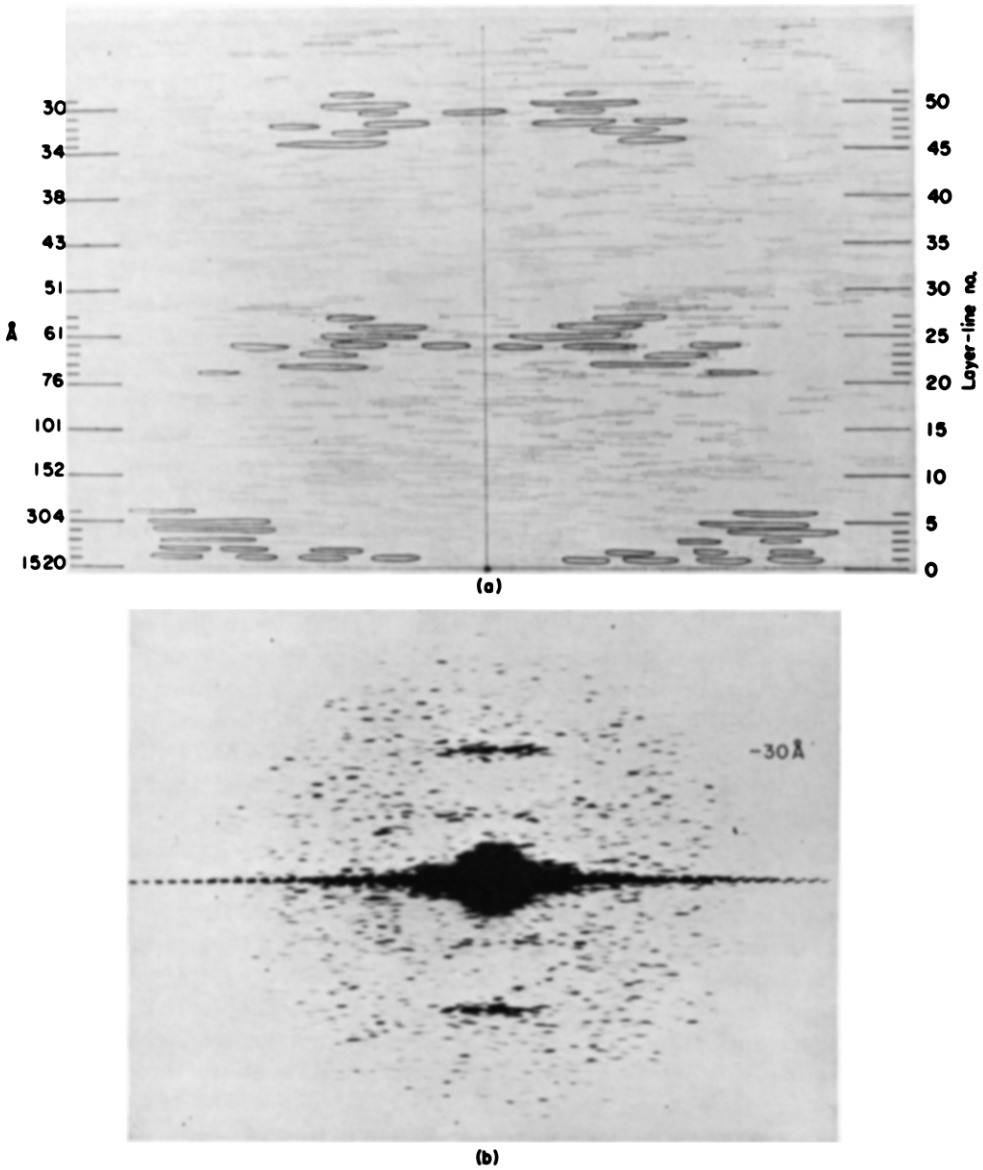

FIG. 2. Transforms of the HbS fiber of Fig. 1(a) obtained by computer (a) and optically (b). (a) An array of densities corresponding to the area outlined was transformed on a Nova computer and the output displayed by a high-speed printer as integers corresponding to increasing amplitude levels. Maxima that were determined to be members of the reciprocal lattice of the fiber are outlined in black to aid in visualization. Layer-lines on which maxima have been identified are indicated by hatch marks on the right axis. (b) Optical transform. Distances (in Å) refer to corresponding spacings along the fiber axis.

reflections representing five and three-start helical families (Crepeau *et al.*, 1977). After measuring the location of the maxima in a number of transforms, however, it became clear that the fiber structure could not be so simple since reconciliation of the transform with a single reciprocal lattice was impossible. Measurements showed that the 1/30 Å maxima were always too far from the equator to fit onto any lattice line connecting an equatorial reflection with a 1/60 Å reflection. This was a puzzling observation until we decided to try to increase the length of fiber transformed, while maintaining the same transform size by averaging data points together. With the improved technique of fiber preparation from stirred HbS solutions, we were able to find several sufficiently straight fibers to double our sampling length. The effect on the computed transform was dramatic in terms of enhancement in signal/noise and an increased separation of layer-lines due to a decreased sampling frequency. Each of the regions of the transform containing a conspicuous maximum proved to consist of several closely spaced layer-lines, with many of the layer-lines containing multiple maxima (Fig. 2(a)). However this development created a new problem. Instead of not being able to reconcile the maxima with any reciprocal lattice, we were then confronted with the problem of deciding which of the many conceivable lattices was correct. We first tried to interpret the transform by using it to produce filtered images.

Two-dimensional filtered images are produced by masking the transform (setting the Fourier coefficients of areas of the transform equal to zero) and computing an inverse transform. Figure 3 shows a series of filtered images. Figure 3(a) is the digitized, unfiltered image. As expected, when all areas of the transform but the maxima on the layer-lines are masked out, an image with a strong resemblance to the observed fibers is produced (Fig. 3(b)). For the image in Figure 3(c) the maxima on layer-lines 21 to 51 were also filtered out. Because these maxima contained the information necessary to show the location of HbS molecules, this image represents an idealized helix in which the filaments are continuous. (This image is important for the REFORM procedure to be discussed below.) It was hoped that by including only those maxima from one side of the meridian a one-sided image would be produced that would reveal the structure of the fibers. As can be seen in Figure 3(d), even though it is an accurate representation of the filaments on the near-side of the helix, the overlap of density from filaments at various radii makes the image extremely difficult to interpret. Therefore, we turned to three-dimensional Fourier reconstructions in the hope that they would permit us to deduce the structure.

Unlike two-dimensional filtering, which does not require knowledge of the Bessel orders of the maxima, three-dimensional Fourier reconstruction requires that the investigator knows the indexing involved. For simple helical structures, this information can usually be readily obtained by conventional lattice building. For structures which yield complicated transforms, such as seen in Figure 2, this information may not be so readily ascertained. Theoretically, the orders of the maxima could be calculated from a comparison of the phases in transforms which have been computed from views of a fiber which has been rotated about its axis by a small angle on the tilting stage of the electron microscope (Finch, 1972). This was attempted, but there was a marked deterioration of the fiber structure following the first exposure as indicated by an examination of the transforms. The relative intensities of maxima were altered, and there were several anomalous phase changes in pairs of maxima arising from opposite sides of the helix, and thus known to have the same Bessel order. Certain qualitative interpretations, however, could be made. First, all maxima on one side of the meridian in

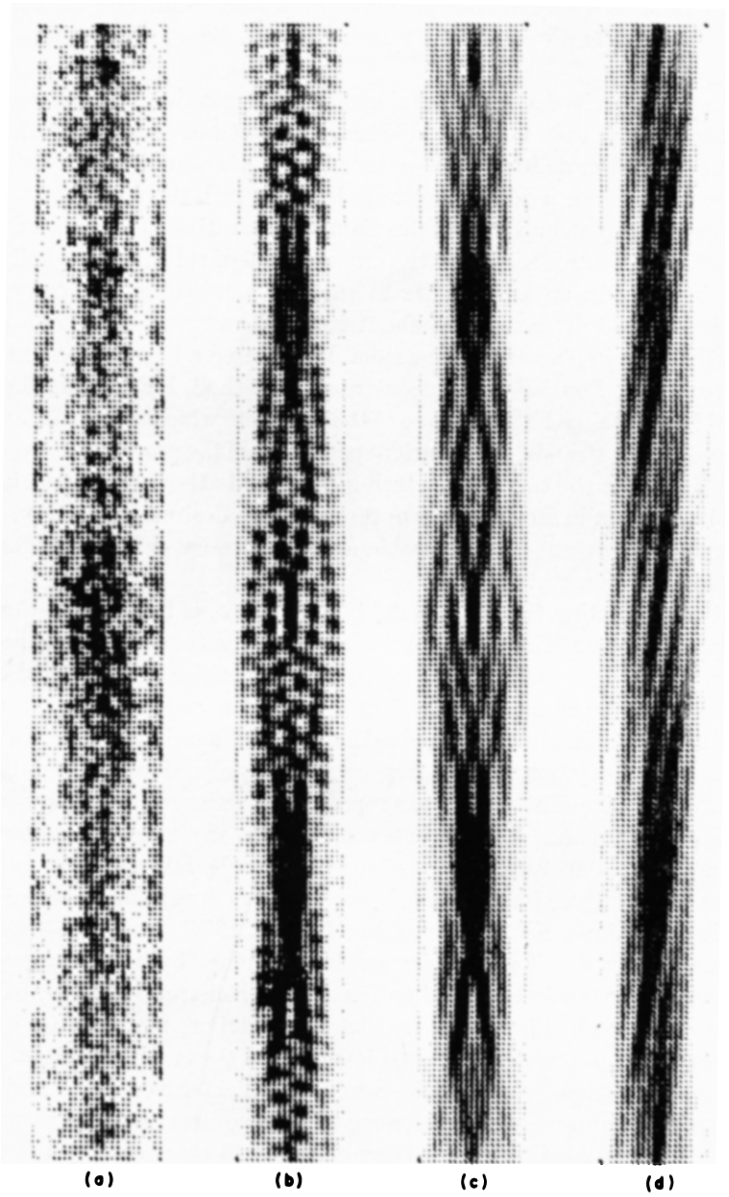

FIG. 3. (a) Digitized image (23 × 216 array) corresponding to the area outlined in Fig. 1(c). (b) Filtered image produced by an inverse transform of the maxima on all the layer-lines. Maxima on the equator, which help define the boundary of the fiber, are also included. (c) Filtered image produced by an inverse transform of the maxima on layer-lines 1 to 6. This image emphasizes the stranded appearance of the fiber. (d) Same as (c) but with maxima on the right side of the meridian excluded. This is an image of the near side of the helix but it is still confusing due to contributions of density from filaments at various radii. Images were recorded from a Tektronix graphics terminal employing a 62 level grey scale.

the equatorial region arose from the same side of the helix, since all phases changed in the same direction. Second, the multiple maxima of a layer-line appeared to be of the same order. Finally, there was generally an increase in Bessel order through the first six layer-lines.

Since the indexing arrived at by examining tilted specimens was incomplete, we sought an alternative method that would provide more quantitative assignments. We concentrated our efforts on deducing the nature of the near-equatorial maxima. These maxima arise from the strandedness of the helix: that is, if the filaments of HbS were replaced by continuous strings having the diameter of an HbS molecule, the transform would be unchanged in this region. If the cross-section of this idealized helix could be determined, it would be an easy matter to generate a helical model, compute transforms of it before and after rotation about its axis, and thus determine the Bessel orders by the change in phase of the maxima. We devised a heuristic technique which we call the real-space Fourier-space reconstruction method, REFORM. The first step of REFORM is to obtain a filtered image of the structure which represents an idealized helix with continuous strands. The Fourier-space stage of the procedure is accomplished by applying a mask to the transform which includes only the near-equatorial maxima (layer-lines 1 to 6). An inverse transform produces the desired image (Fig. 3(c)), and at the same time filters out a considerable amount of noise, which adversely affects algebraic reconstruction methods.

The effect of generating the fiber model in Figure 3(c) is to reduce a three-dimensional problem (the overall fiber structure) to a two-dimensional problem (the structure of a cross-section) since cross-sections taken at any position are identical except for rotation about the central axis. Figure 3(c) is a two-dimensional image, a projection in a plane of the three-dimensional idealized helix, and it consists of a matrix of density points. A row of density points, then, represents the projection of a two-dimensional cross-section onto a line. The set of rows represents a series of projections from many different angles. The change in angle between different views can be computed knowing the distance of a 360° turn of the helix, which can be fairly accurately estimated by inspection of the filtered images. This image was then used as input to the real-space reconstruction technique, EFIRT (Crowther & Klug, 1974). In Figure 4(a) the cross-section is initialized to a uniform density and is surrounded by an annular region of zero density. Figure 4(b) is the first approximation of the reconstruction generated by modifying the cross-section in Figure 4(a) by "back-projecting" the densities in a one-dimensional projection (a row of the filtered image) onto the two-dimensional array. For successive approximations, the densities are back-projected vertically, and the cross-section is rotated counterclockwise between successive iterations. In Figure 4(c) the cross-section has been modified by 54 rows of data and rotated a total of 90°. When 108 rows (representing a 180° rotation of the filaments) are included, the reconstructed image is complete, indicating that the idealized helix (Fig. 3(c)) has 2-fold rotational symmetry. Figure 4(d) shows the result of the REFORM process. It is immediately evident that there are 14 filaments arranged in a hexagonal fashion. Some difference in the intensities of the strands are presumably due to negative staining effects. With this information we computed the image expected from a helix with that cross-section, and its transform was virtually identical to the fiber transforms in the equatorial region. The model image was rotated, transformed again, and the order of the maxima determined by dividing the change in phase of each maximum by the angle of rotation. The orders are 2, 4, 6, 8, 10 and 12 for layer-lines 1, 2, 3, 4, 5 and 6, respectively.

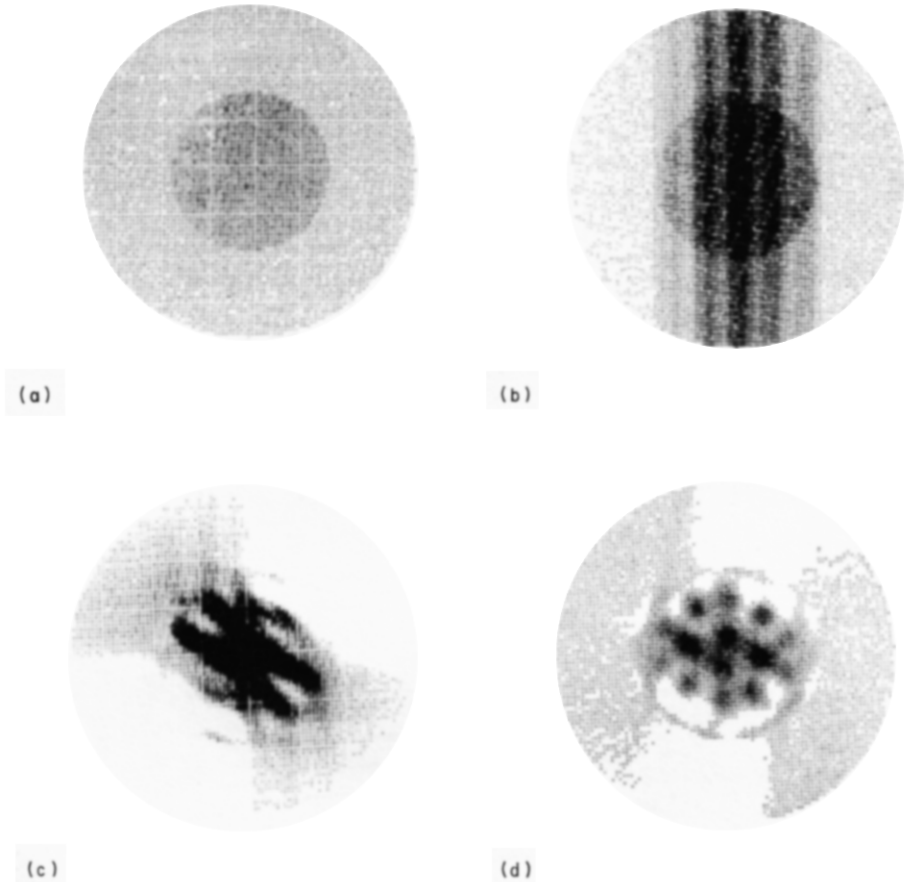

FIG. 4. Cross-section of helical image of Fig. 3(c) as calculated by REFORM and displayed on the graphics terminal. (a) Initialization of reconstruction space to a uniformly dense cross-section surrounded by an annulus of zero density. (b) First approximation made by back-projecting a 1-dimensional projection onto the 2-dimensional array. (c) Half-completed reconstruction including 54 iterations of the REFORM algorithm. For each iteration a row of data in the filtered image is used to adjust the previous approximation by back-projection. The image is then rotated $360/n$ degrees, where n is the number of rows that corresponds to a 360° rotation of the filaments. In this case, n is equal to 216. (d) Final approximation after back-projection of half of the 1-dimensional projections of the cross-section available in the filtered image of Fig. 3(c). The image has been rotated a total of 180°.

With the orders of the equatorial region confirmed, it became a simple matter to determine the order of higher resolution maxima by constructing the logical lattices. In addition to the Bessel orders of layer-lines 1 to 6, the Bessel order of layer-line 49 can be confidently assigned. Since the maximum is on the meridian, it must have order 0. Midway between layer-line 1 and layer-line 49, with Bessel orders of 2 and 0, respectively, is layer-line 25, which is therefore assigned a Bessel order of 1. Similarly, layer-line 26 is assigned a Bessel order of 3, lying on a lattice line connecting layer-line 3 with a Bessel order of 6, and layer-line 49 with Bessel order 0. Proceeding in this manner, all the maxima can be unambiguously assigned the proper Bessel orders. The assignments are summarized in an n, l plot in Figure 5.

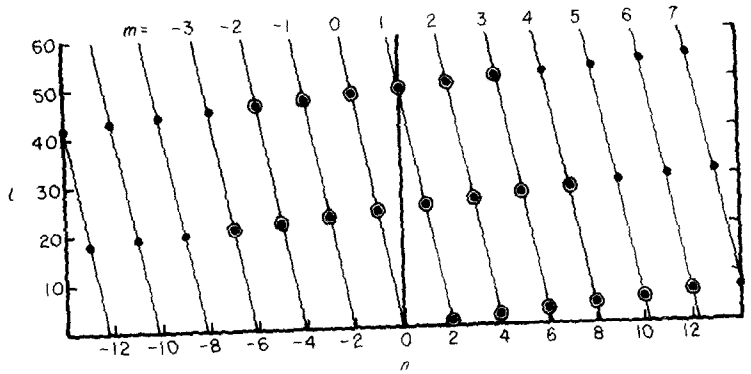

FIG. 5. n, l plot for the selection rule $l = -24n + 49m$. Lines are drawn through points of constant m. Co-ordinates where maxima have been conclusively identified in the transforms of fibers (a), (b) and (c) are circled.

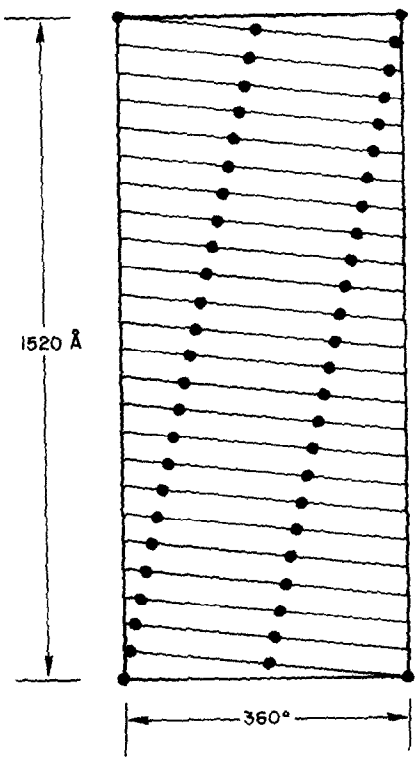

FIG. 6. The helical net of the basic 1-start helix described by the selection rule $l = -24n + 49m$. There are 49 asymmetric units in the 24 turns of an axial repeat. Each asymmetric unit consists of 7 HbS molecules.

The selection rule linking the layer-lines to their Bessel orders for fiber (a) is $l = -24\,n + 49\,m$, where l is the layer-line number, n is the Bessel order, and m is any integer which satisfies the equation (Klug *et al.*, 1958). The coefficient of n (-24) is the number of turns of the basic one-start helix per axial repeat, the negative sign indicating that the sense of this helix is left-handed. The coefficient of m (49) is the number of asymmetric units per axial repeat (see Fig. 6). Each unit of the basic helix consists of seven HbS molecules. Since the repeat distances for the three fibers are slightly different, their selection rules differ, and hence the layer-line numberings vary from fiber to fiber. The general selection rule is $l = -[(u-1)/2)]n + um$, where u, the number of helical subunits per axial repeat, is equal to the number of the layer-line with the zero order maximum. The value of u was determined for each transform by a least-squares fit of the observed layer-line spacings. For fibers (a), (b) and (c), u was determined to be 49, 59 and 45, respectively.

Fourier–Bessel synthesis using layer-lines 1 to 6 was performed with the result as

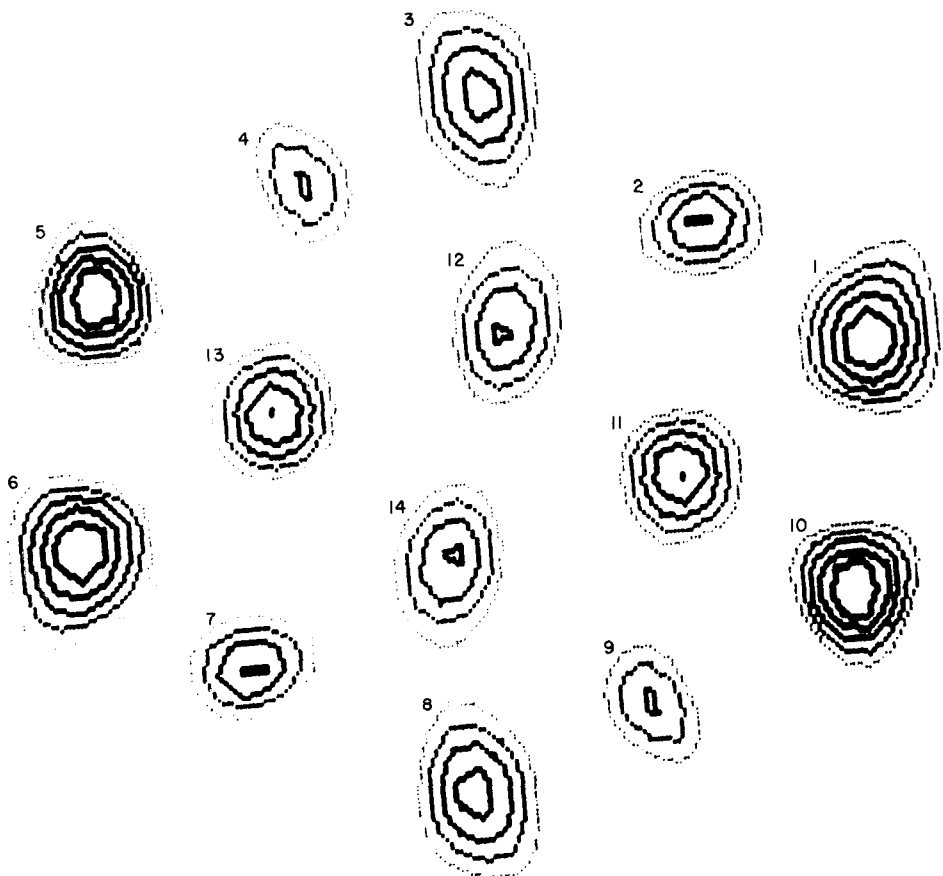

FIG. 7. Fourier–Bessel synthesis using layer-lines 1 to 6, producing a reconstruction corresponding to the cross-section of the idealized helix of Fig. 3(c) and the REFORM image of Fig. 4(d). The filaments are numbered for easy reference.

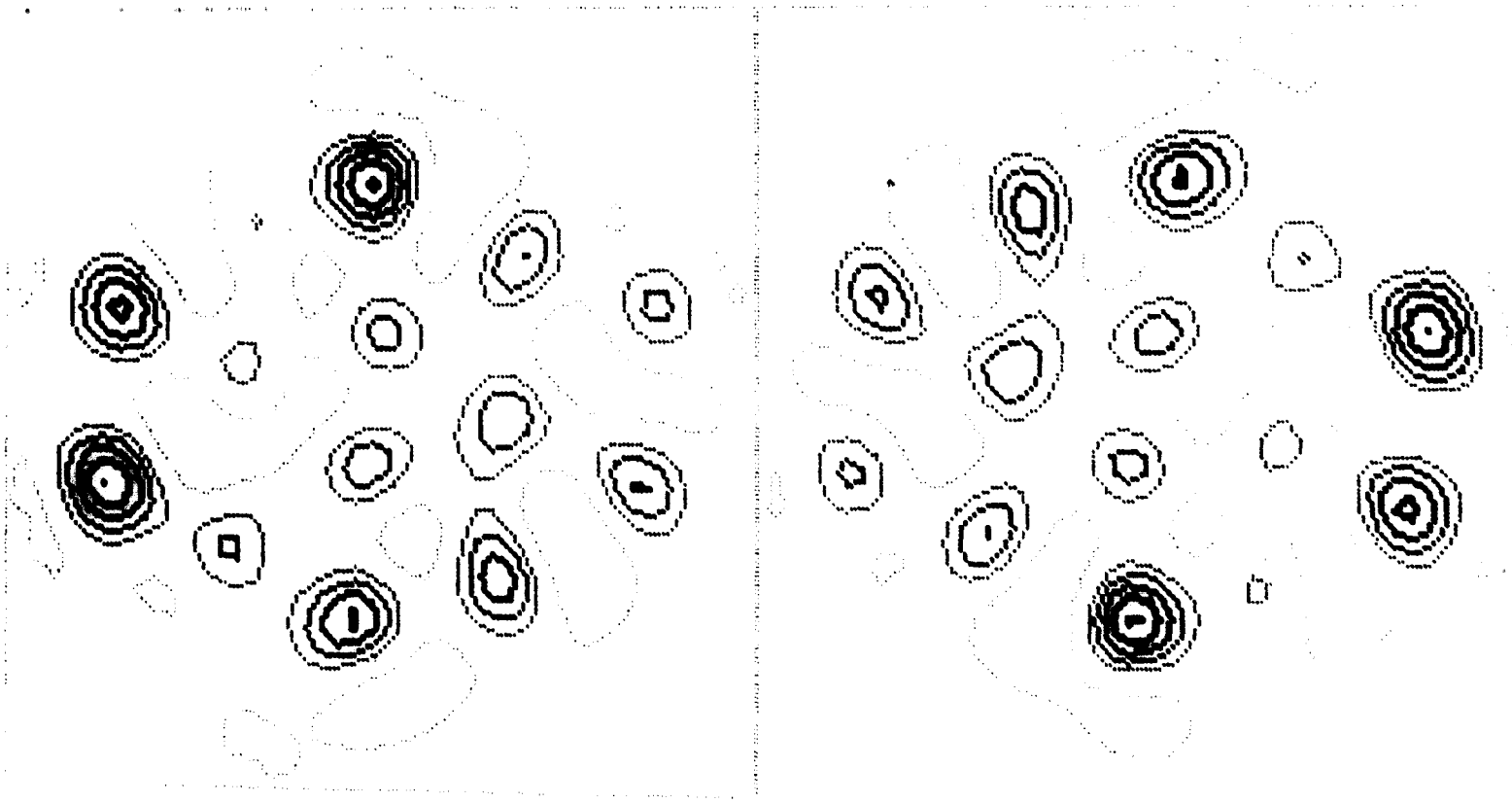

FIG. 8. Fourier–Bessel synthesis using all layer-lines to define the location of individual molecules. The 2 cross-sections are 30 Å apart, therefore filaments which are strongly represented in one are very weak in the other, since the diameter of HbS is roughly 60 Å. In a series of closely spaced sections the location of HbS molecules within each filament can be deduced.

shown in Figure 7. No attempt has been made to define accurately the boundary between protein and stain in this and subsequent reconstructions, since our only concern at this stage is in defining the position of the filaments and locating the HbS molecules within them. Without layer-lines 21 to 51 to define the location of individual molecules, each filament is more or less equally represented. The elliptical cross-section that produces the variable diameter in two-dimensional projection is readily apparent. It can also be seen that this is the result of the arrangement of the filaments in a roughly hexagonal fashion. There is an apparent 2-fold rotation axis perpendicular to the plane of the cross-section, due to the presence of only even Bessel functions on the layer-lines included, so there are seven types of filaments. Filaments 1 and 6, which are identical, are quasi-equivalent to filaments 5 and 10, and filaments 2 and 7 are quasi-equivalent to filaments 4 and 9, since they would be equivalent if there was a perfectly hexagonal matrix.

When all the layer-lines are included in the reconstruction, density varies from filament to filament in a cross-section depending on the location of the HbS molecules within each filament. By observing the density of each filament in a series of cross-sections (Fig. 8), the relative locations of HbS molecules within each filament can be deduced. Since the filaments lie at a variety of radii, a simple surface lattice cannot be drawn, but if the lattice of each type of filament is projected radially onto the outermost surface lattice, the result can be graphed as in Figure 9. The major helical

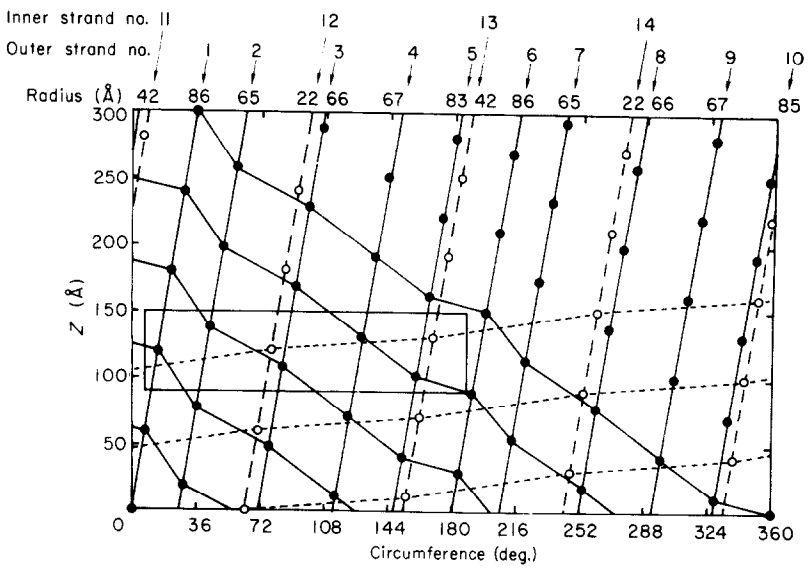

FIG. 9. Surface lattice formed by a radial projection of the 14-stranded structure. The 14 filaments are displayed with a numbering system corresponding to the designations in Fig. 7. For each filament the center of its radial distance (corrected for flattening) is indicated at the top. The outer 10 filaments are represented by solid circles and the inner 4 filaments by open circles. The inner 4 filaments occur at 2 pairs of radii such that a pseudo 1-start helix (broken lines) has a slope which alternates between 2 angles, which differ slightly, at each intersection with an inner filament. The uncertainties in assignment are ± 2 Å within a filament, $\pm 2°$ angular location of filaments, and ± 3 Å radial spacing on the basis of standard deviations of the averages of reconstructions of 5 fibers. The rectangular box delineates one asymmetric unit.

families are indicated with solid lines for the ten exterior filaments and broken lines for the interior four. The locations of the HbS molecules have been determined by averaging values observed in individual reconstructions with the result that each center of a molecule is positioned along its filament with an uncertainty of less than ± 2 Å (less than the size of the points on the Figure). A solid sphere model of the structure is presented in Figure 10.

In addition to the predominant fibers, we have also observed the two minor forms shown in Figure 11. The "diamondback" structure of Figure 11(a) is easily recognized

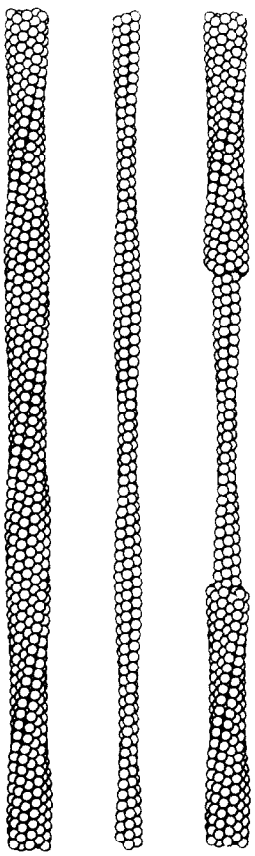

FIG. 10. Solid sphere models of the helical elements of the fibers of HbS. The models present the outer filaments (on the left); the inner filaments (in the center) in alignment with the outer filaments such that the narrow diameter region of the inner filaments corresponds to the narrow diameter region of the outer filaments; and a cutaway version (on the right) showing both inner and outer filaments in proper juxtaposition.

by its repeating pattern of diamond shapes. The smaller fiber in Figure 11(b) has a characteristic "zig-zag" pattern which indicates a lack of 2-fold symmetry. Both forms were analyzed by REFORM. The diamondback fiber was found to be composed of ten filaments and the zig-zag fiber to be composed of six filaments. In one case a 12-filament fiber lacking only one of the outer pairs was observed. The arrangement of filaments

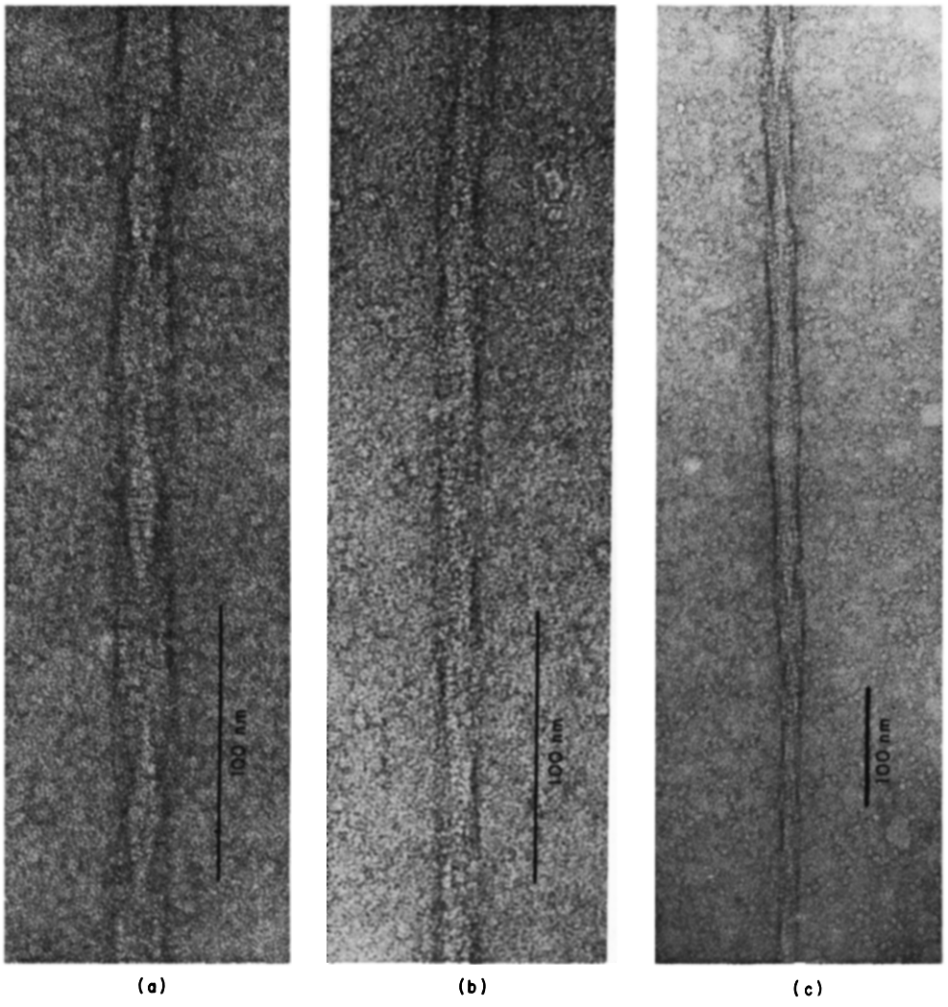

FIG. 11. (a) A minor form of HbS fiber occasionally seen and readily recognized by the regularly recurring diamond-shaped pattern. (b) Another minor form of HbS fiber seen occasionally. Opposite sides of the fiber are clearly inequivalent, indicating a lack of 2-fold symmetry. (c) A single fiber which exhibits normal form and the 2 forms ((a) and (b)) in different regions. REFORM indicates that the minor forms could be formed by the loss of filaments from the normal form.

in each is the same as that seen if one strips away some of the filaments from the 14-stranded structure. Indeed, since these variants are usually found in fibers which also have regions of normal 14-stranded structure (Fig. 11(c)), it would appear that it is the loss of filaments during grid preparation that leads to these forms. A hypothetical pathway of filament loss is depicted in Figure 12. The loss of filaments 1, 2, 6 and 7 produces the 10-stranded structure. The further loss of filaments 3, 4, 5 and 13 results in a fiber with six filaments and a triangular cross-section. There appears to be no relation between this six-stranded structure and that described by Finch *et al.* (1973).

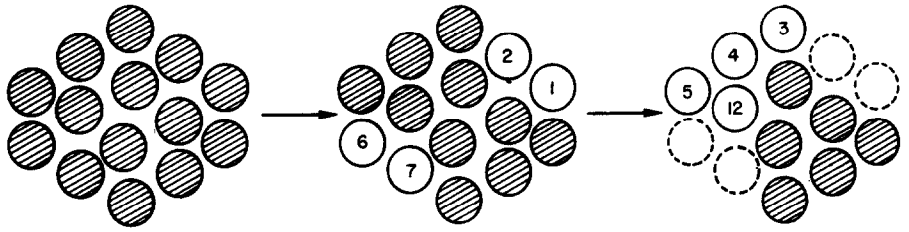

FIG. 12. Hypothetical formation of 2 minor forms of HbS fibers from the predominant 14-stranded structure. The equivalent filament pairs 1–2 and 6–7 are missing in the 10-stranded structure. With the further loss of filaments 3, 4, 5 and 12, the 6-stranded fiber of Fig. 11(b) is formed. (It could also be the loss of the equivalent filaments 8, 9, 10 and 11.)

4. Discussion

Since a helix is a structure that can be constructed from just a single type of molecule with each one residing in an equivalent environment, a surprising aspect of the HbS fiber structure is that the filaments are arranged in a roughly hexagonal fashion. Since there is a local 2-fold screw axis, seven of the filaments are distinct. Thus, there are seven possible environments in which an HbS molecule might reside and a different set of neighboring contacts for each unique filament. Since some contacts would necessarily be weaker than others, this would seem to indicate that closest packing is a more important consideration for the overall stability of the helix than an equivalent intermolecular bonding pattern for all HbS molecules. This is not the first structure for which non-hollow hexagonal packing has been reported. The seven-stranded cable of glutamine synthetase (Frey *et al.*, 1975) has a hexagonal cross-section, but the single interior filament does not disturb the equivalent contacts of the six other filaments. Preliminary observations (C. W. Akey & G. W. Dykes, unpublished data) indicate that a form of phosphorylase b can be identified that is composed of a large number of filaments packed in a hexagonal matrix. It would appear that the advantages of hexagonally packed filaments (Pauling & Corey, 1953; Crick, 1953) are demonstrated in these fibers.

There is ample evidence that the 14-stranded fibers are the predominant structures in both hemolysates and sickled cells. Cross-sections of sickled cells, embedded cells and bundles show the presence of non-hollow elliptical fibers with similar features to those obtained for the 14-stranded fibers (Garrell *et al.*, 1979). The high density of HbS gels observed by Ross *et al.* (1977) can also be explained by the packing observed in these fibers, which seems to maximize the quantity of protein within a helical configuration. In studies of sickled cells lysed with negative stain, of which one of the fibers in this study is an example, occasional cells would absorb the negative stain but remain largely intact. By the criteria of visual appearance and optical diffraction, there was no difference between the fibers within the intact cells and those released by lysis. This arrangement of molecules within the fibers also supplies a rationale for the extremely co-operative nature of fiber formation (Hofrichter *et al.*, 1974; Malfa & Steinhardt, 1974; Moffat & Gibson, 1974). Since the unit cell of the fiber is large and involves a variety of contacts, it seems reasonable that formation of the fiber is dependent on the formation of a large and complex nucleus.

An effort to extend the structural analysis of the fiber to higher resolution is under

way. However, the information relevant to subunit location and stereochemistry of contacts is split among many weak maxima with intensities near noise level, so it will require the comparison and averaging of many transforms to obtain accurate reconstructions. These reconstructions will answer the question of whether there will be little similarity among the sets of contacts for the seven types of filaments, or whether there will be a type of quasi-equivalence. Several lines of evidence concerning the nature of the contacts are already available. Roughly similar orientations of the molecular axes are likely since polarization studies indicate that the molecular x-axes of HbS are within 22° of the fiber axis (Hofrichter *et al.*, 1973). Within this constraint, however, there is great latitude for variability, including the inversion of polarity of some filaments such as that present in the structure of HbS crystals seen by Wishner *et al.* (1975). The number of surface mutations that have been found to influence sickling is growing (Bookchin *et al.*, 1967; Bookchin & Nagel, 1971,1974; Kraus *et al.*, 1972; Benesch *et al.*, 1976,1977). This would seem to favor the concept of a large number of different intermolecular contacts. The fact that the repeat distance varies from fiber to fiber indicates that, in addition to there being a number of contacts, small shifts in at least some of the contacts are allowed, implying a certain amount of nonspecificity. An analysis of the minor forms of fibers seen in our micrographs sheds some light on the relative strength of a few of the inter-filament bonding regions. Two pairs of filaments are weakly bound to the central core, since they are absent in the diamond-back fiber (see Fig. 12). The central pair of filaments may be an integral feature of the fibers, since it is found in all three forms, i.e. the 14-, 10- and 6-filament structures.

The structures of the 6- and 10-filament forms suggest a possible bonding pattern for the hemoglobin S molecules in the fibers with elements of quasi-equivalence that would greatly reduce the number of classes of intermolecular contacts. This pattern is summarized in Figure 13 and involves arrangement of the individual filaments in pairs. The filaments within pairs are related by a 2-fold screw axis, as has been found for crystals of hemoglobin S (Wishner *et al.*, 1975). It has also been suggested that a similar arrangement may apply to the fibers (Wishner *et al.*, 1976; Magdoff-Fairchild & Chiu, 1979). As indicated in Figure 13, the 14-filament fibers can be viewed as seven-filament pairs organized around the central pair. The spacing along the fiber axis of the HbS molecules in the central pair (see Fig. 9) is exactly "half-staggered", in agreement with the arrangement of filament pairs in the crystals (Wishner *et al.*, 1975). Within the limits of our measurements (± 2 Å) the spacing of the two pairs involving positions 5 to 13 and 10 to 11 (in the notation of Fig. 8) is also half-staggered. However, the spacings of the remaining four pairs agree less well with the half-staggered arrangement, with deviations in the range of 6 to 8 Å from the 30 Å half-staggering for pairs 1–2, 3–4, 6–7 and 8–9. These deviations appear to be significantly larger than the uncertainties in the assignments of positions of molecules along the filaments (Fig. 9). Additional data at higher resolution will be required to determine whether the two types of pairs, exactly half-staggered and nearly half-staggered, resemble the pairs in the crystals. Issues of filament polarity must also be considered, both within pairs and between pairs. Within the filament pairs observed in crystals a parallel structure occurs (while orientation between adjacent pairs is anti-parallel), but there is as yet no direct evidence that the pairing scheme proposed in Figure 13 necessarily involves parallel filaments. In addition, even with parallel alignment of filaments within pairs, some sets of pairs, such as 6–7 and 1–2 (which are most readily lost in disassembly) could be anti-parallel with respect to the other filaments in the structure.

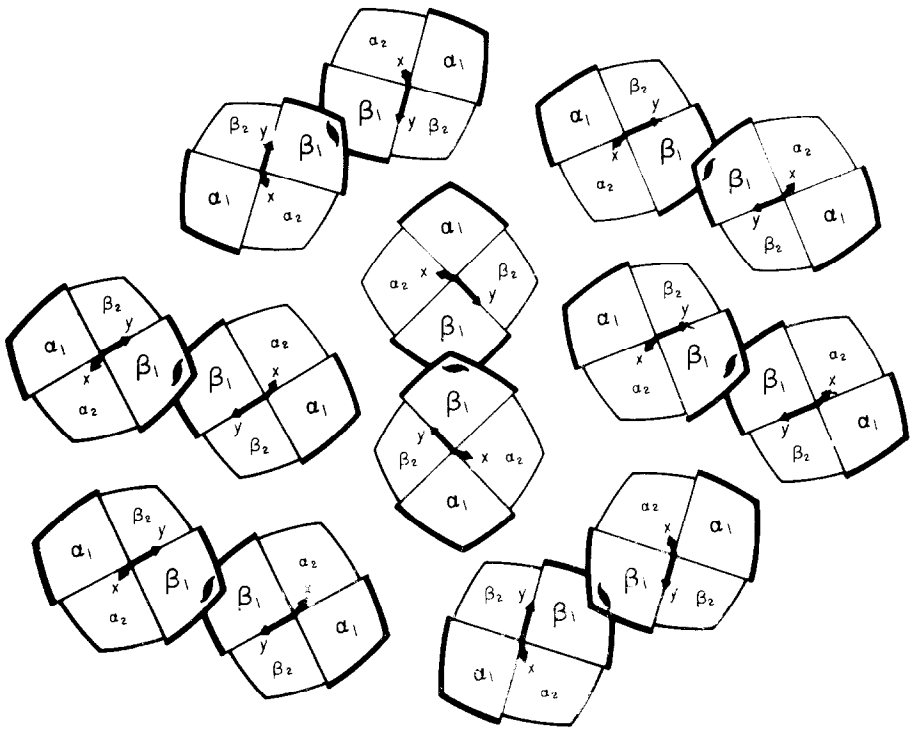

FIG. 13. Possible molecular orientations of the hemoglobin S molecules. The x and y molecular axes for the molecules in the arrangement suggested by the quasi-equivalence involving filament pairs are given for each location. For each pair of molecules the position of the screw axis is indicated.

An attractive feature of a filament-pairing model along the lines proposed in Figure 13 is that it specifies within narrow limits the stereochemistry of the intermolecular contacts. The β-6 site lies between filaments within the pairs, along with the β-73 site also implicated in fiber formation (Wishner *et al.*, 1976). The β-121 and α-23 sites lie between molecules of the same filament while the sites on the α chains in the vicinity of α-47, implicated in fiber formation by Benesch *et al.* (1976), would lie at the contacts within and between filament pairs. The filament pairing scheme would also have possible implications for fiber assembly. Linear arrays of filament pairs could assemble through weak interactions in a low-order association process, followed by co-operative assembly of the pairs into the fibers. Since there are seven pairs of filaments, a relationship may exist between this number and the reaction order for gelation kinetics corrected for non-ideality (Hofrichter *et al.*, 1974,1976; Ross *et al.*, 1977).

The fact that the fibers may be constructed with paired filaments of molecules in an arrangement close to the one found in crystals raises an interesting question concerning the formation of the fibers. It has been thought that sickle-cell fiber structure was dependent on the Glu → Val transition, but it may be that this change merely further stabilizes a structure that is already marginally stable. Although we have never detected such a structure in HbA, Finch *et al.* (1973) show a micrograph of a fiber found

from a lysed deoxygenated normal erythrocyte that bears a striking resemblance to these 20 nm fibers.

This work was supported by U.S. National Science Foundation (grant BMS74 00012), the National Institutes of Health (HL-13591, GM-07273 and CA-14454) and the National Foundation–March of Dimès (1–611).

We thank C. Akey for helpful discussions and help in detecting the partially disassembled fibers, and Drs B. Magdoff-Fairchild, J. Finch and M. Perutz for valuable comments on an earlier version of this paper.

REFERENCES

Benesch, R. E., Yung, S., Benesch, R., Mack, J. & Schneider, R. G. (1976). *Nature (London)*, **260**, 219–221.

Benesch, R. E., Kwong, S., Benesch, R. & Edalji, R. (1977). *Nature (London)*, **269**, 1977.

Bertles, J. F., Rabinowitz, R. & Dobler, J. (1970). *Science*, **169**, 375–377.

Bookchin, R. M. & Nagel, R. L. (1971). *J. Mol. Biol.* **60**, 263–270.

Bookchin, R. M. & Nagel, R. L. (1974). *Seminars in Hematol.* **11**, 577–595.

Bookchin, R. M., Nagel, R. L. & Ranney, H. M. (1967). *J. Biol. Chem.* **242**, 248–255.

Crepeau, R. H., Dykes, G. & Edelstein, S. J. (1977). *Biochem. Biophys. Res. Commun.* **75**, 496–502.

Crepeau, R. H., Dykes, G., Garrell, R. L. & Edelstein, S. J. (1978). *Nature (London)*, **274**, 616–617.

Crick, F. H. C. (1953). *Acta Crystallogr.* **6**, 589–697.

Crowther, R. A. & Klug, A. (1974). *Nature (London)*, **251**, 490–492.

DeRosier, D. J. & Moore, P. (1970). *J. Mol. Biol.* **52**, 355–369.

Dykes, G., Crepeau, R. H. & Edelstein, S. J. (1978). *Nature (London)*, **272**, 506–510.

Eklundh, J. O. (1972). *IEEE Transactions on Computer*, July, pp. 801–803.

Finch, J. T. (1972). *Proc. 6th European Congr. Electron Microscopy*, pp. 578–579.

Finch, J. T., Perutz, M. F., Bertles, J. F. & Dobler, J. (1973). *Proc. Nat. Acad. Sci., U.S.A.* **70**, 718–722.

Frey, T. G., Eisenberg, D. & Eiserling, F. A. (1975). *Proc. Nat. Acad. Sci., U.S.A.* **72**, 3402–3407.

Garrell, R. L., Crepeau, R. H. & Edelstein, S. J. (1979). *Proc. Nat. Acad. Sci., U.S.A.*, **76**, 1140–1144.

Gordon, R., Bender, R. & Herman, G. T. (1970). *J. Theor. Biol.* **29**, 471–481.

Hofrichter, J., Hendricker, D. G. & Eaton, W. A. (1973). *Proc. Nat. Acad. Sci., U.S.A.* **70**, 3604–3608.

Hofrichter, J., Ross, P. D. & Eaton, W. A. (1974). *Proc. Nat. Acad. Sci., U.S.A.* **71**, 4864–4868.

Hofrichter, J., Ross, P. D. & Eaton, W. A. (1976). *Proc. Nat. Acad. Sci., U.S.A.* **73**, 3035–3039.

Josephs, R. & Borisy, G. (1972). *J. Mol. Biol.* **65**, 127–155.

Josephs, R., Jarosch, H. S. & Edelstein, S. J. (1976). *J. Mol. Biol.* **102**, 409–426.

Klug, A., Crick, F. H. C. & Wycoff, H. (1958). *Acta Crystallogr.* **11**, 199–213.

Kraus, L. M., Miyaji, T., Iuchi, I. & Kraus, A. P. (1972). *Biochemistry*, **11**, 3576–3582.

Magdoff-Fairchild, B. & Chiu, C. C. (1979). *Proc. Nat. Acad. Sci., U.S.A.*, **76**, 223–226.

Malfa, R. & Steinhardt, J. (1974). *Biochem. Biophys. Res. Commun.* **59**, 807–893.

Moffat, K. & Gibson, Q. H. (1974). *Biochem. Biophys. Res. Commun.* **61**, 237–242.

Ohtsuki, M., White, S. H., Zeitler, E., Wellems, T. E., Fuller, S. D., Zwick, M., Makinen, M. W. & Sigler, P. D. (1977). *Proc. Nat. Acad. Sci., U.S.A.* **74**, 5538–5542.

Pauling, C. & Corey, R. B. (1953). *Nature (London)*, **171**, 59–61.

Pumphrey, J. G. & Steinhardt, J. (1976). *Biochem. Biophys. Res. Commun.* **69**, 99–105.

Ross, P. D., Hofrichter, J. & Eaton, W. A. (1977). *J. Mol. Biol.* **115**, 111–134.

Stetson, C. A. (1966). *J. Expt. Med.* **123**, 341–345.

White, J. G. (1968). *Blood*, **31**, 561–579.

Williams, R. C. & Fisher, H. W. (1970). *J. Mol. Biol.* **52**, 121–123.

Wishner, B. C., Ward, K. B., Lattman, E. E. & Love, W. E. (1975). *J. Mol. Biol.* **98**, 179–194.

Wishner, B. C., Hanson, J. C., Ringle, W. M. & Love, W. E. (1976). *Proc. Symp. Mol. Cell. Aspects of Sickle Cell Disease*, pp. 1–31. DHEW Publication no. (NIH) 76–1007. Bethesda, Maryland.